Single Image Reconstruction using Novel Super Resolution Technique for Large Scaled Images

Ramanath Datta
ST. THOMAS College of Engineering and Technology
Sekhar Mandal
Indian Institute of Engineering Science and Technology
Saiyed Umer (saiyedumer@gmail.com)
Aliah University https://orcid.org/0000-0002-1476-041X
Ahmad Ali AlZubi
King Saud University
Abdullah Alharbi
King Saud University
Jazem Mutared Alanazi
King Saud University

Research Article

Keywords: Super resolution, Sparse representation, Prediction model, Image reconstruction

Posted Date: November 23rd, 2021

DOI: https://doi.org/10.21203/rs.3.rs-1047644/v1

Single Image Reconstruction using Novel Super Resolution Technique for Large Scaled Images

Ramanath Datta[a], Sekhar Mandal[b], Saiyed Umer[c], Ahmad Ali AlZubi[d], Abdullah Alharbi[d], Jazem Mutared Alanazi[d]

[a]*Department of Electronics & Communication Engineering, St.Thomas' College of Engineering and Technology, Kolkata, India*
[b]*Department of Computer Science & Technology, Indian Institute of Engineering Science and Technology, Shibpur, Kolkata, India*
[c]*Department of Computer Science & Engineering, Aliah University, Kolkata, India, Email:saiyedumer@gmail.com*
[d]*Computer Science Department, Community College, King Saud University, Saudi Arbia*

Abstract

A fast and novel method for single-image reconstruction using super resolution (SR) technique has been proposed in this paper. The working principle of proposed technique has been divided into three components. In the first component, a low resolution image is divided into several homogeneous or non-homogeneous regions. This partition is based on the analysis of texture pattern within that region. Only the non-homogeneous regions undergo to the sparse representation for super resolution image reconstruction in the second component. The obtained reconstructed region from the second component undergoes to a statistical based prediction model to generate its more enhanced version in the third component. The remaining homogeneous regions are bicubic interpolated and reflected to the required high resolution image. The proposed technique is applied on some Large scaled Electrical, Machine and Civil architectural design images. The purpose of using these images is that these images are huge in size and processing such large images for any applications, is time consuming. The proposed SR technique results the better reconstructed SR image from its very lower version with low time complexity. The performance of the proposed system on the Electrical, Machine and Civil architectural design images is compared with the state-of-the-art methods and it is shown that the proposed system outperforms the other competing methods.

Keywords: Super resolution, Sparse representation, Prediction model, Image reconstruction

1. Introduction

A high resolution image is always desirable in the most applications of digital image processing such as office automation, medical imaging, remote sensing and video surveillance. A high resolution image gives better appearance and better classification of image regions. The image resolution means the scene area represented by a single pixel and higher resolution (HR) refers to small area resulting in more spatial image details. This resolution of an image depends on the camera device used during image acquisition. There are various issues to obtain high resolution image using hardware devices. However, algorithmic image reconstruction based techniques are more promising for obtaining HR image from low resolution (LR) ones.

Suppressing the degradation introduced during image acquisition and increasing the high frequency components, we may get the HR images from observed LR images. The process is referred to as Super Resolution (SR) technique. Moreover, during SR process, the non-redundant information contained in LR images are combined with domain specific knowledge to create HR image. One of the commonly used approach to SR is single image interpolation, which is used to increase the image size. In this case, no additional information is provided and hence, the quality of the HR image is limited due to the nature of the problem. We adopt here patch based (or exemplar based) method for SR, where a LR image I_L is partitioned into several patches and then each LR patch is replaced by its corresponding HR patch to reconstruct HR image, say, I_H. Various methods differ mainly due to: how to partition I_L into LR patches, how to generate or select HR patch corresponding to a given LR patch, and how to combine HR patches to reconstruct I_H.

The objective of this problem domain is to obtain the best possible SR image and to accept the SR image as quickly as possible. The solution to this problem is depend upon available single LR image or multiple LR images. So, the methods of SR technique are categorized into single frame SR and multi-frame SR techniques. Moreover, the single-frame SR algorithm is also categorized into two approaches: (a) interpolation based method and (b) patch based method [15].

The most of these methods use the single-frame & the patch based super resolution techniques for reconstruction of HR images from LR images. These methods have achieved better performance in the research area of image super resolution. From the great success of this single-frame & patch based SR method [26], in this paper patches are extracted from the input image I. Then the implementation focuses on the recovering SR version of the given low-resolution version of I. To capture the significant co-occurrence prior and to speed up the process here we obtain some representation from the image patch pairs extracted from HR and LR images. This representations are the first and second order gradients from each patch.

The contributions of the proposed work are as follows:

- To speedup the SR image reconstruction, the LR patches are classified into two groups, namely, homogeneous and non-homogeneous. If a LR patch belongs to non-homogeneous group then sophisticated SR method is applied to obtain a HR patch; otherwise bi-cubic interpolation method is applied to obtain HR patch.

- LR patches are classified by an unsupervised method, i.e., k-means clustering technique based on the texture features computed from the gray-level co-occurrence matrices of the image patches.

- In training phase, the features extracted from LR and HR patch pair of I_L and I_H undergo a sparse representation to generate Dictionary. We have adopted this sparse representation using Dictionary, as recent result suggests that the linear relationships of HR signals are well recovered from their lower dimensional projection obtained from sparse representation. Moreover, image patch based sparse representation plays an important role for regularizing SR ill-posed problem with effectiveness and robustness properties.

- The obtained HR image patches are fed to a prediction model to produce a refined SR image patches.

The organization of this paper is as follows: Section 2 discusses some related works. Section 3 describes the proposed method with detailed discussion of each components of the proposed system. The experimental results and discussions have been demonstrated in Section 4. Section 5 concludes this paper.

2. Related Work

The interpolation based methods such as Bilinear or Bicubic interpolation applied on smooth images with some jagged and ringing artifacts to exploit the natural image prior that results better results [6][21]. The patch based methods capture the prior of co-occurrences between LR and HR image patch pairs locally. Then it employees a large database of LR and HR patch pairs, and uses a learning mechanism for corresponding mapping between the LR and HR image patches that are applied to a new LR image to reconstruct its most likely HR version [26][9]. Generally, these methods are based on the image edge prior or image gradient prior [21]. The objective of this kind of method is to magnify the image in such a way that the edge sharpness and the texture details within the image are preserved. Natsui & Nagao [16] proposed a single-frame SR technique using multiple graph structured programs based on Cartesian Genetic Programming which is one of the evolutionary method like genetic algorithms. Lai et al. [13] proposed a method for single-frame SR technique, where a total variation regularization was used to minimize the iterative back-projection based SR reconstruction error by suppressing the chessboard and ringing artifacts at the time of acquiring the high resolution image. Dang & Radha [7] proposed a single image SR technique using Tangent Space Learning of high resolution patch manifold which is based on the linear approximation of HR patch space using sparse subspace clustering algorithms. A method for compressed sensing reconstruction method with single plane wave transmission for super resolution of ultrasound images had been proposed by Shu et al. [20]. A multi-frame SR technique based on the fusion of multiple low resolution images captured at VW & NIR lighting conditions with different camera positions for synthesizing HR color images had been proposed by Honda et al. [10]

A well comprehensive survey for super resolution of biometric images such as face (2D+3D), iris, fingerprint and gait based on operation domain (spatial & frequency), singe-frame & multi-frame, reconstruction & learning and feature domain & deep-learning based SR techniques had been discussed by Nguyen et al. [17]. Akyol & Gö Kmen [2] have proposed a method for face super resolution by enhancing the shape and texture information of faces. A multi-channel constraints based image super resolution techniques which has the capability for collaborative representations, clustering, multilayer mapping relationships to reconstruct HR images from LR images had been proposed by Cao & Li [4]. Zhao et al. proposed a method for SR technique where the adaptive sparse coding had been employed by establishing the regularization parameters with integrating correlation and sparsity terms in the regularization [29]. Their SR method modulates the collaborative representation and the sparse representation.

3. Proposed Methodology

The proposed super resolution (SR) technique is applied mainly to reconstruct the high resolution (HR) image from the low resolution (LR) image of electrical circuit drawings using single-frame and patch based super resolution technique. The proposed method can also be applied to other drawings such as mechanical drawing and architectural drawing. We have done some experiments in this direction to see the performance of the proposed method.

The proposed method has three main phases: (i) In the first phase, we partition m-training images I_Ls into number of patches and then the patches are divided into two clusters based on the homogeneous/non-homogeneous texture pattern using k-means clustering algorithm. Then classification of a LR patch of an individual LR image I_L is done by comparing its GLCM texture features with that of the cluster centers; (ii) In the second phase, the bicubic interpolation [12] (i.e. no super resolution is applied on it) is applied on the homogeneous patches, while the non-homogeneous patches undergo for sparse representation based SR method followed by statistical prediction model based algorithms; (iii) Here the color image I is transformed to its (Y, C_b, C_r) color channel and only luminance channel (Y) is used in the first and second phase. The remaining C_b, C_r channels are interpolated using bi-cubic interpolation technique and are combined with the obtained HR Y-channel in the third phase. A brief overview of the proposed system is shown in Fig. 1.

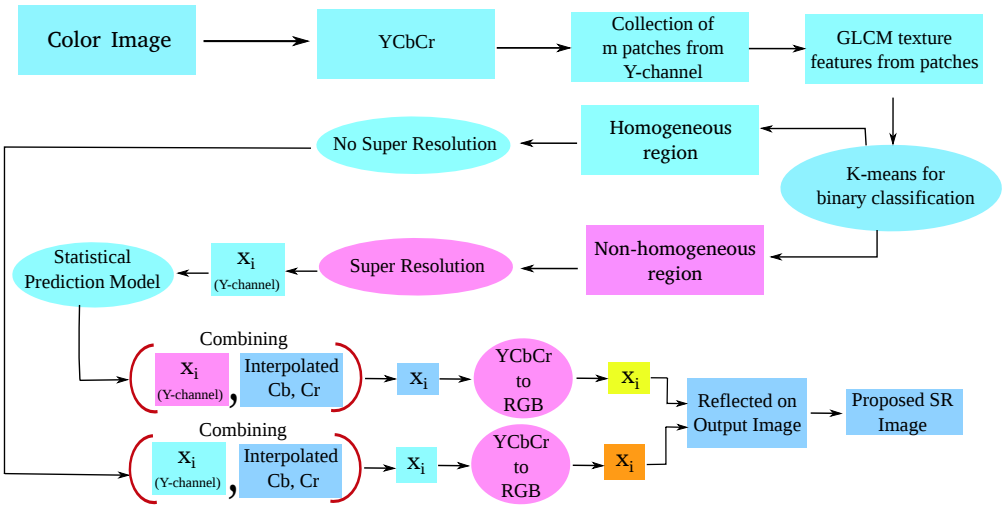

Figure 1: Data flow diagram of the proposed system.

3.1. Preprocessing

During preprocessing, (R, G, B) of each input image I_L is transformed to (Y, C_b, C_r) color channel, and super resolution is performed only on Y-channel LR image to obtain Y-channel HR image. Here we have employed patch based SR technique. Hence, a patch $w_{n\times n}$ with overlapping of p pixels both the horizontal and vertical directions is considered from $\mathcal{I}_Y$. Then GLCM texture features [24] $\mathcal{F}_{w_i} \in \mathbb{R}^{d\times 1}$ is computed from each w_i

i.e. $\mathcal{I}_Y$ gives $(\mathcal{F}_{w_1}, \cdots, \mathcal{F}_{w_N}) \in \mathbb{R}^{d \times N}$, where N be the number of patches and d is the number of texture features from each patch. Now k-means clustering algorithm is applied on GLCM texture features collected from m-training $\mathcal{I}_Y$ images to obtain a code-book $C \in \mathbb{R}^{d \times 2}$ considering two classes ($k = 2$): homogeneous and non-homogeneous. For a given image $\mathcal{I}_Y$, the feature vector $\mathcal{F}_{w_i} \in \mathbb{R}^{d \times 1}$ corresponding to each w_i is compared with $C \in \mathbb{R}^{d \times 2}$ using minimum distance classifier to predict whether w_i has homogeneous or non-homogeneous region. The non-homogeneous w_i is considered as LR (y_i) and undergoes for super resolution technique. In the next section, we discuss super resolution technique using sparse representation.

3.2. SR using sparse representation (Case-1)

Sparse representation is a powerful technique for representing, compressing, and processing of high dimensional signals in low dimensional space. The classes of signals such as images and audios can be modelled through sparse representation with respect to their fixed bases. The effective and efficient convex optimization or greedy pursuit algorithms are available for computing those representation with high fidelity. These are the main reasons for successful and wide use of sparse representation [25]. So, the sparse representation has extensive used in many computer vision tasks, such as image super resolution, image de-noising, image impainting, motion and data segmentation, image classification, and face recognition. In most of these applications, using sparsity as prior, sparse representation outperforms the state-of-the-art results.

In this work, we have employed patch-based sparse representation for single image super resolution (SR). However, non-overlapping patch-wise operation may cause block artifacts; hence, to overcome this problem, overlapping patches are employed. The sparse representation provides high quality image reconstruction for SR algorithms by using overlapping patches over the image [23]. On the other hand, overlapping patches leads to more time consumption. To overcome this, we have adopted only small overlap between patches. To reduce computational cost further we have employed a technique for patch selection based on its homogeneous or non-homogeneous texture pattern (discussed above) and applied the sparse representation only on those patches that are non-homogeneous. During sparse representation, we consider LR patches (y_i) from Y-channel of LR image $\mathcal{I}_y$ and then extract features from each y_i.

In the training phase, more precisely during Dictionary learning, we take high resolution (HR) image, say, $\mathcal{I}_x$ from the application domain and deliberately form its low resolution (LR) version, say, $\mathcal{I}_y$ through appropriate down-sampling method. If $\mathcal{I}_x$ is a graylevel image, so is $\mathcal{I}_y$. However, if we had to handle color images, then consider that $\mathcal{I}_x$ and $\mathcal{I}_y$ are corresponding Y-channel images. Different features can be extracted from the LR patches which are mentioned in the existing literature. Freeman et al. [8] extracted edge based information from LR patches by using high pass filter. Chang et al.[5] and Yang et al.[26] have extracted first and second order gradients from LR and HR patches. In this work, we also use first ($g_1 = [-1, 0, 1], g_1^T$) and second order ($g_3 = [1, 0, -2, 0, 1], g_3^T$) gradients of patches. These filters are directly applied on the training images (LR $\mathcal{I}_y$ and HR $\mathcal{I}_x$) which yields four gradient maps at each location. Then any patch is represented in terms of feature

vector corresponding to its gradient map. To track the correspondence between HR (obtained original image) and LR patches (down-sampled image), feature vectors of x_i and y_i are concatenated to form v_i.

The above mentioned feature vectors are used to create two dictionaries $\mathcal{D}_l$ and $\mathcal{D}_h$ corresponding to LR and HR patches respectively which will be subsequently exploited to obtain sparse representations of LR and HR patches, respectively.

Since sparse representation is an ill-posed problem, to solve this problem we take the help of constraints. First, image observation model is considered where a low resolution image $\mathcal{I}_y$ is obtained from the given high resolution image $\mathcal{I}_x$, such that

$$\mathcal{I}_y = \mu \mathcal{H} \mathcal{I}_x \tag{1}$$

where μ is the down-sampling factor and $\mathcal{H}$ is the blurring filter. Since Eq. (1) represents a many-to-one mapping, for a given low resolution image $\mathcal{I}_y$ infinitely many solutions of $\mathcal{I}_x$ can be obtained by solving Eq. (1). To resolve this issue, we consider that each patch $x \in \mathcal{I}_x$ can be represented as a sparse linear combination of dictionary $\mathcal{D}_h$. Similar concept is true for $y \in \mathcal{I}_y$ also. Or, in general, the vector v (= $[x \mid y]$) can be represented by a sparse combination of dictionary $\mathcal{D}$, which in turn would be concatenation of $\mathcal{D}_h$ and $\mathcal{D}_l$, i.e., $\mathcal{D} = \mathcal{D}_h \mid \mathcal{D}_h$. The vector v contains various features including pixel intensities of HR and LR patches concatenated together. Hence,

$$v = \mathcal{D}\alpha \tag{2}$$

for some coefficient vector $\alpha \in R^K$, where K is the number of words or elements in the Dictionary and $\|\alpha\|_0 \leq\leq K$, which is a sparsity constraint. Note that both $\mathcal{D}$ and α are unknown and are learned simultaneously by optimizing the following equation.

$$\min \|\alpha\|_0 \;\; \textit{such that} \;\; \|\mathcal{D}\alpha - v\|_2^2 \leq \epsilon \tag{3}$$

Thus the above mentioned [Eq. (3)] sparse representation α corresponds to both HR and LR patches together, which have spatial compatibility between the neighbors. So using this α for x, the entire HR image $\mathcal{I}_x$ is regularized and refined using the reconstruction constant. For this purpose, a local modeling for sparsity prior has been introduced for local patches to recover some HR patch x which may be lost during processing.

During local modeling the HR patch x_i is derived for the corresponding LR patch y_i. For these two dictionaries $\mathcal{D}_l$ and $\mathcal{D}_h$ are needed separately. Recall that dictionary $\mathcal{D}$ is generated, through sparse model of the patches, from vector v (= $[x \mid y]$). This suggests that dictionary $\mathcal{D}$ can straightaway be decomposed into $\mathcal{D}_l$

and $\mathcal{D}_h$. Also note that here both these dictionaries $\mathcal{D}_l$ and $\mathcal{D}_h$ have the same sparse representation α (i.e. α_l or α_h are same) for each y_i and x_i patch pairs. And this suggests the method for generating HR patch, given the test LR patch and two dictionaries. For each input LR patch y_i, the corresponding sparse representation α is obtained based on $\mathcal{D}_l$. Now the patch bases of $\mathcal{D}_h$ are combined according to α to generate high resolution patch x_i. This solution may be mathematically formulated as

$$\min \|\alpha\|_0 \;\; \textit{such that} \;\; \|\mathcal{D}_l\alpha - \mathfrak{F}y\|_2^2 \leq \epsilon \tag{4}$$

where $\mathfrak{F}$ is the feature extraction operator includes intensity mapping of the patch along with first and second order spatial derivatives of the patch. Solving Eq. (4) we obtain a α to represent y in terms of the dictionary $\mathcal{D}_l$. Now same α is used to generate x_i based on $\mathcal{D}_h$. So we have

$$x = \mathcal{D}_h\alpha \tag{5}$$

The problem defined in Eq.(4) is NP-hard problem [1] and it says that the obtained sparse representation α could be sufficiently sparse. This can be efficiently approximated by introducing l_1-norm in place of l_0 norm as follows:

$$\min \|\alpha\|_1 \;\; \textit{such that} \;\; \|\mathcal{D}_l\alpha - \mathfrak{F}y\|_2^2 \leq \epsilon \tag{6}$$

Now, the regularization parameter is introduced in Eq. (6) to obtain following loss function

$$\mathcal{J}(\alpha) = \min_{\alpha} \|\mathcal{D}_l\alpha - \mathfrak{F}y\|_2^2 + \lambda\|\alpha\|_1 \tag{7}$$

Here the term λ balances the sparsity of the solution and fidelity of the approximation to y. The formulation in Eq. (7) is Lasso [27] optimization problem, which is a linear regression regularization with l_1-norm on α. In this work for SR image we obtain corresponding HR patches to only those LR patches which are non-homogeneous region. So, during processing each non-homogeneous region is considered as y_i image and then a patch slides in raster scan, i.e., horizontally and then vertically. So, there may be possibility of overlapping patches for ambiguous region. So, to check closely the previously computed HR patch x_i from the SR reconstruction $\mathcal{D}_h\alpha$ of y, we modify the Eq.(7) as follows:

$$\min \|\alpha\|_1 \;\; \textit{such that} \;\; \|\mathcal{D}_l\alpha - \mathfrak{F}y\|_2^2 \leq \epsilon \,, \;\; \|\mathfrak{P}\mathcal{D}_h\alpha - w\|_2^2 \leq \epsilon \tag{8}$$

where w contains the value for the particular reconstructed HR image on overlap and $\mathfrak{P}$ is a matrix for overlap region between the target patch and the previously computed HR patch. The optimization in Eq.(8) is formulated

as

$$\min_{\check{\alpha}} \|\hat{\mathcal{D}}\check{\alpha} - \hat{y}\|_2^2 + \lambda\|\check{\alpha}\|_1 \tag{9}$$

where $\hat{\mathcal{D}} = [\mathcal{D}_l, \beta\mathfrak{P}\mathcal{D}_h]^T$ and $\hat{y} = [\mathfrak{F}y, \beta w]^T$. The parameter $\beta = 1$ is the control of trade-off between the matching of LR input y and finding a HR patch x which is compatible with its neighbor. The final optimal solution of Eq.(9) is $\check{\alpha}$ and the final HR patch $\check{x}$ is computed as

$$\check{x} = \hat{\mathcal{D}}\check{\alpha} \tag{10}$$

The HR patch $\check{x}$ obtained from Eq. (10) has much more better resolution then the LR patch y.

3.3. SR using prediction model (Case-2)

Now the obtained HR patch $\check{x}$ undergoes a predicted model which generates much higher resolution HR patch $\hat{x}$ considering the previously obtained $\check{x}$ as LR patch y. Here also two dictionaries $\mathcal{D}_l$ and $\mathcal{D}_h$ have been used. The objective of this prediction model is to predict the missing HR details for each LR patch y (here $y = \check{x}$) via $\mathcal{D}_l$ and $\mathcal{D}_h$, having different elements. Then a statistical prediction model is being utilized for prediction the HR representation vector α_h of each patch from its corresponding α_l. In above Case-1 technique the sparse coefficient α is similar for $\alpha_l = \alpha_h$. To introduce more sparsity in α_l, $\mathfrak{z}_l \in \{-1, 1\}^{m_l}$ is computed from α_l which is as follows

$$\mathfrak{z}_{l,j} = \begin{cases} 1, & \alpha_{l,j} > \rho, \forall\, j = 1, \cdots, m_l \\ 0, & \text{otherwise} \end{cases} \tag{11}$$

where ρ is a threshold which adaptively changes for each LR patch and is computed based on following criterion $\sum_{j=1}^{m_l} |\alpha_{l,j}|^2$ for $(|\alpha_{l,j} \leq \rho|) \leq n\lambda^2$, where λ is a pre-specified parameter. So, the sparsity patterns $\mathfrak{z}_l = \{-1, 1\}^{m_l}$ for LR patch and $\mathfrak{z}_h = \{-1, 1\}^{m_h}$ for the HR patch capture the relationships between these two patterns and for this a statistical prediction model is required which is described in the following section.

To capture the statistical dependencies within the sparsity pattern $\mathfrak{z}_l = \{-1, 1\}^{m_l}$ and $\mathfrak{z}_h = \{-1, 1\}^{m_h}$, the restricted Boltzmann machine (RBM) [22] technique is employed which may be described by the conditional probability [18] as follows:

$$p(\mathfrak{z}_h/\mathfrak{z}_l) = \frac{1}{y} exp(b_h^T \mathfrak{z}_h + \mathsf{z}_h^T \mathcal{W}_{hl} \mathfrak{z}_h) \tag{12}$$

where $b \in \mathbb{R}^m$ is the bias vector and $\mathcal{W} \in \mathbb{R}^{m_h \times m_l}$ is an interaction matrix between $\mathfrak{z}_l = \{-1, 1\}^{m_l}$ and $\mathfrak{z}_h = \{-1, 1\}^{m_h}$. Thus

$$p(\mathfrak{z}_h/\mathfrak{z}_l) = \prod_{j=1}^{m_h} \phi((b_{h,j} + \mathbf{w}_{h_l}^T \mathfrak{z}_l)\mathfrak{z}_{h,j}) \tag{13}$$

where $\phi(s) = \frac{1}{(1+exp(-2s))}$ is the sigmoid function and is due to the elements of $\mathfrak{z}_h$ which are statistically independent of $\mathfrak{z}_l$. Basically, RBM is an exponential model works with binary vectors and it leads to the conditional marginal probability for each elements of $\mathfrak{z}_h$ in $\mathfrak{z}_l$ such that

$$p(\mathfrak{z}_{h,j} = 1/\mathfrak{z}_l) = \phi(b_{h,j} + \mathbf{w}_{h_l}^T \mathfrak{z}_l), \quad \forall j = 1, \cdots, m_h \tag{14}$$

The obtained $\mathfrak{z}_h$ is employed to compute the HR co-efficient α_h using α_l based on the below criterion:

$$\alpha_{h,j} = \{ \begin{array}{ll} \mathcal{G}_j, & \mathfrak{z}_{h,j} = 1 \\ 0, & \mathfrak{z}_{h,j} = -1 \end{array} \tag{15}$$

where $\mathcal{G} \in \mathbb{R}^{m_h}$ is the Gaussian distribution, i.e., $\mathcal{G}\alpha_l \sim N(\mathcal{C}_{hl}\alpha_l, \sum_{hl})$, where $\mathcal{C}_{hl} \in \mathbb{R}^{m_h \times m_l}$ and $\sum + ml \in \mathbb{R}^{m_h \times m_h}$. This leads to the following conditional expectation:

$$E[\alpha_{h,j}|\mathfrak{z}_{h,j} = 1, \alpha_l] = \mathfrak{c}_{hl}^T \alpha_l, \forall j = 1, \cdots, m_h \tag{16}$$

The models defined in Eq.(15) and (16) show the linear mapping of α_l to α_h and it happens when $\mathfrak{z}_h$ is known. In case where reletion between α_l and $\mathfrak{z}_l$ is nonlinear, then the final estimate of α_h using α_l, $\mathfrak{z}_h$, $\mathfrak{z}_l$ may be given by an MMSE estimator as follows:

$$\begin{aligned} \hat{\alpha}_{h,j} &= E[\alpha_{h,j}|\mathfrak{z}_l, \alpha_l] \\ &= \sum_{\mathfrak{z}_h \in \Gamma_j} E[\alpha_{h,j}|\mathfrak{z}_h, \mathfrak{z}_l, \alpha_l] P(\mathfrak{z}_h|\mathfrak{z}_l, \alpha_l) \\ &= \sum_{\mathfrak{z}_h \in \Gamma_j} E[\alpha_{h,j}|\mathfrak{z}_{h,j} = 1, \alpha_l] P(\mathfrak{z}_h|\mathfrak{z}_l)) \\ &= E[\alpha_{h,j}|\mathfrak{z}_{h,j} = 1, \alpha_l] P(\mathfrak{z}_{h,j} = 1|\mathfrak{z}_l)) \\ &= (\mathfrak{c}_{hl}^T \alpha_l) \phi(b_{h,j} + \mathbf{w}_{h,j}^T \mathfrak{z}_l) \end{aligned} \tag{17}$$

From the above MMSE estimator (Eq. (18)), the obtained α_h is not only sparse but also leads to better signal recovery [18]. Moreover, MMSE estimator [3] can be represented as a product of linear terms with respect to α_l and a nonlinear term with respect to $\mathfrak{z}_l$. The final predicted HR patch x is given by

$$x = \mathcal{D}_h \hat{\alpha_h} \tag{18}$$

3.4. Initial validation of proposed methods

Since we are more acquainted with natural images (or scenes) the above discussed super resolution (SR) techniques (both Case-1 and Case-2) are applied on generic images like Butterfly, Girl, Pepper, Starfish and

Zebra as shown in Fig. 2. The effect of SR technique using sparse representation (Case-1) is shown in Fig. 3; whereas that of SR technique using sparse representation followed by prediction model (Case-2) are shown in Fig. 4. Moreover, the performance is also shown in Table 1 in terms of Peak Signal to Noise Ratio (PSNR) and Structural Similarity Index (SSIM) [11] indexes. The Table shows that the performance of Case-2 is much better than Case-1.

Note that the collection of HR and LR patch pairs, collected from natural image pairs, undergoes dictionary learning process to obtain $\mathcal{D}_l$ and $\mathcal{D}_h$. For this learning we have employed the parametric dictionary learning discussed in [26] and [18].

Figure 2: Some Generic HR images.

Figure 3: Result of the proposed SR technique using sparse representation.

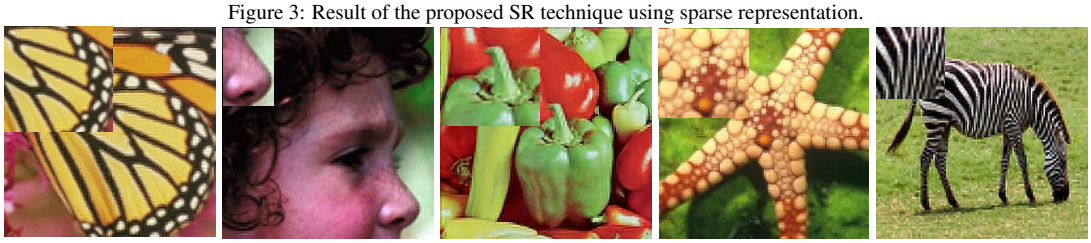

Figure 4: Result of the proposed SR technique using sparse representation followed by prediction model.

Table 1: Comparative performance for Case-1 and Case-2 SR techniques for generic images using PSNR and SSIM.

	Butterfly	Girl	Pepper	Starfish	Zebra
Case-1	32.92	41.97	34.04	35.39	31.02
	0.8751	0.9579	0.8380	0.9148	0.6839
Case-2	35.74	45.01	34.89	38.83	31.48
	0.9412	0.9754	0.8772	0.9605	0.7344

4. Experimental results

This section presents and evaluated the performance of proposed SR techniques when applied on engineering drawing (i.e., line drawing) images in general, and electrical circuit drawings in particular.

4.1. Data used

For the proposed single image SR technique, we demonstrate the results on some Electrical circuit, Machine layout and Civil architectural design images which are originally captured in high resolution camera. These images are huge in size and the use of these images for any application is computationally time consuming on moderate capacity machines. To speedup the process, we keep only its lower version (i.e. down-sampled version) and apply the proposed super resolution (SR) techniques whenever required. Fig. 5 shows the original version of the Electrical circuit images (Img_1, Img_2, Img_3, Img_4, Img_5, Img_6, Img_7, Img_8), Machine layout and Civil architectural design images (Img_9, Img_{10}, Img_{11}, Img_{12}, Img_{13}, Img_{14}, Img_{15}, Img_{16}). Table 2 provides the size of these images in terms of $(Rows) \times (Columns) \times (Channels)$. We have applied the proposed method on these images and have obtained the performance. These images are large scaled images and huge in size. To make the system understandable, convenient and comparable with the other state-of-the-art methods, we have manually cropped a small region from these images (shown in Fig.5) and considered them as original HR images and then down-sampled each cropped region to its lower resolution images (shown in Fig.5).

Table 2: Description for employed Image names and their sizes.

Name	Size	Name	Size
$Img1$	$1700 \times 2400 \times 3$	$Img9$	$900 \times 2100 \times 3$
$Img2$	$1650 \times 3050 \times 3$	$Img10$	$600 \times 900 \times 3$
$Img3$	$1850 \times 3600 \times 3$	$Img11$	$600 \times 900 \times 3$
$Img4$	$2200 \times 3300 \times 3$	$Img12$	$1800 \times 2400 \times 3$
$Img5$	$750 \times 1600 \times 3$	$Img13$	$1200 \times 1500 \times 3$
$Img6$	$1100 \times 1700 \times 3$	$Img14$	$750 \times 900 \times 3$
$Img7$	$3500 \times 4900 \times 3$	$Img15$	$2100 \times 3000 \times 3$
$Img8$	$2500 \times 3300 \times 3$	$Img16$	$2400 \times 3600 \times 3$

4.2. Results and discussion

During experimentation, each image I is converted to its (Y, C_b, C_r) color channels. Then only Y-channel of LR image ($\mathcal{I}_y$) is considered to undergo to the proposed algorithm to reconstruct Y-Channel of HR image $\mathcal{I}_x$. Corresponding $\mathcal{I}_{C_b}$ and $\mathcal{I}_{C_r}$ are up-sampled and interpolated to be combined with $\mathcal{I}_x$, and then converted to RGB image. Now a window w_i of size 50×50 slides over $\mathcal{I}_y$ with 50% overlapping of pixels in horizontal and vertical direction picks up the patches of same size. Then GLCM [24] texture features $\mathcal{F}_{w_i} \in \mathbb{R}^{200\times1}$ are extracted from each w_i. The collection of these texture features selected randomly from $m = 5$ training images, are used to obtain a code-book $CB \in \mathbb{R}^{200\times2}$ using k-means clustering algorithm for evaluating the homogeneous and non-homogeneous region for each $w_i \in \mathcal{I}_y$.

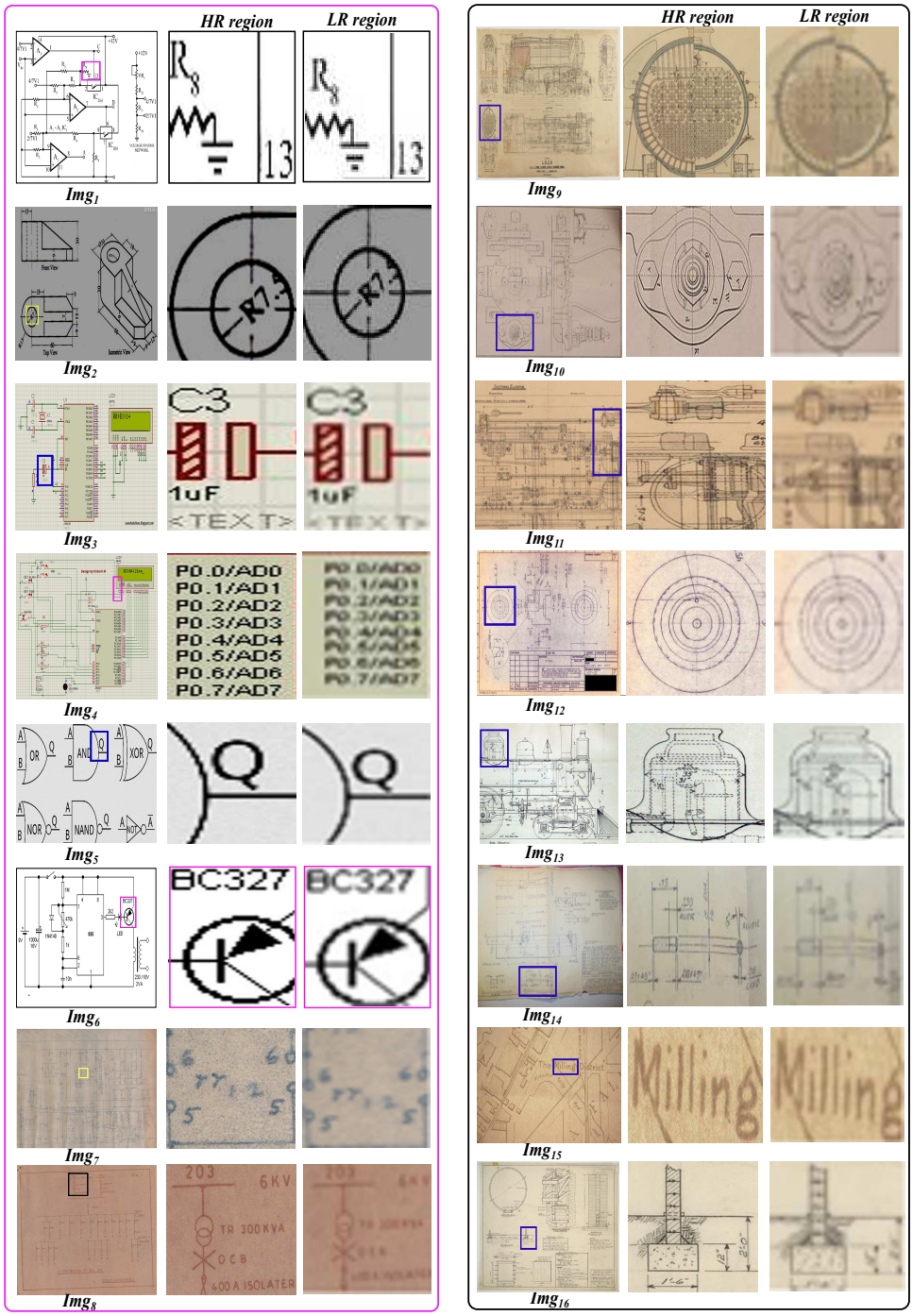

Figure 5: Img_1, Img_2, Img_3, Img_4, Img_5, Img_6, Img_7, Img_8 are large scaled electrical circuit images whereas Img_9, Img_{10}, Img_{11}, Img_{12}, Img_{13}, Img_{14}, Img_{15}, Img_{16} are the large scaled machine and civil layout design images.

Any homogeneous patch w_i does not undergo to the proposed SR technique. It is bicubic interpolated and converted to its RGB version. The up-sampled patches are used to form the high resolution (HR) image. The non-homogeneous patches w_i undergo to the proposed SR technique. Here during super resolution technique

we consider each non-homogeneous patch w_i as a LR image $\mathcal{Y}$ and it's reconstructed SR patch $\mathcal{X}'$ is utilized to form the final HR image. Note that for each non-homogeneous LR region $\mathcal{Y}$, we apply first order gradient (g_1, g_2) and second order gradient (g_3, g_4) features which yield four gradient maps at each location. Then a window $w_{5\times5}$ with 50% overlapping is considered over each feature map of $\mathcal{Y}$. Now, feature vector with respect to each position of $w_{5\times5}$ is extracted from four feature map which are concatenated to obtain a feature vector for $w_{5\times5}$ to obtain its representation as $y_i \in \mathbb{R}^{100\times1}$. Then the joint feature learning technique for the dictionary has been performed on the concatenated HR and LR patch pair features which derives $\mathcal{D}_l \in \mathbb{R}^{25\times K}$ and $\mathcal{D}_h \in \mathbb{R}^{100\times K}$, dictionary for the corresponding HR and LR patch pairs respectively. Here for each dictionary $\mathcal{D}_h$ or $\mathcal{D}_l$, $K = \{512, 1024, 2048\}$ items are considered. During dictionary learning, the color images are transformed from the RGB to YC_bC_r channels and then features are extracted from the corresponding Y-channel only.

The i-th LR patch $\mathcal{Y}_i$ corresponding to the non-homogeneous region is used to obtain it's SR patch by employing the proposed SR technique via sparse representation technique described in Section 3.2. The obtained $\mathcal{X}_i$ undergoes to the statistical prediction model described in Section 3.3. The performance of the proposed SR technique for electrical circuit images Img_1, Img_2, Img_3, Img_4, Img_5, Img_6, Img_7, Img_8 and for machine and civil layout design images Img_9, Img_{10}, Img_{11}, Img_{12}, Img_{13}, Img_{14}, Img_{15} and Img_{16} using the dictionary pairs ($\mathcal{D}_l \in \mathbb{R}^{25\times512}$, $\mathcal{D}_h \in \mathbb{R}^{100\times512}$), ($\mathcal{D}_l \in \mathbb{R}^{25\times1024}$, $\mathcal{D}_h \in \mathbb{R}^{100\times1024}$) and ($\mathcal{D}_l \in \mathbb{R}^{25\times2048}$, $\mathcal{D}_h \in \mathbb{R}^{100\times2048}$) have been shown in Fig. 6 respectively.

Table 3 shows the performance of the proposed system in terms of PSNR (first row for each image) and SSIM (second row for each image) indexes for the images shown in Fig. 6 using the dictionary pairs ($\mathcal{D}_h \in \mathbb{R}^{25\times512}$,$\mathcal{D}_l \in \mathbb{R}^{100\times512}$), ($\mathcal{D}_h \in \mathbb{R}^{25\times1024}$, $\mathcal{D}_l \in \mathbb{R}^{100\times1024}$) and ($\mathcal{D}_h \in \mathbb{R}^{25\times2048}$, $\mathcal{D}_l \in \mathbb{R}^{100\times2048}$) respectively.

Table 3: Performance of the reconstructed SR image using the proposed system with respect to PSNR and SSIM indexes.

	Img_1,	Img_2,	Img_3,	Img_4,	Img_5,	Img_6,	Img_7,	Img_8
$D_h \in \mathbb{R}^{512\times100}$	33.82	40.52	32.64	31.22	31.56	31.17	32.65	32.85
	0.8792	0.9197	0.8991	0.9287	0.9135	0.9149	0.9191	0.9372
$D_h \in \mathbb{R}^{1024\times100}$	35.82	42.52	34.38	33.40	33.52	32.31	32.47	35.08
	0.8791	0.9298	0.8784	0.9181	0.9296	0.9203	0.9290	0.9191
$D_h \in \mathbb{R}^{2048\times100}$	40.84	46.52	39.89	38.63	38.89	37.59	36.51	40.11
	0.9994	0.9999	0.9987	0.9982	0.9915	0.9928	0.9990	0.9991
	Img_9,	Img_{10},	Img_{11},	Img_{12},	Img_{13},	Img_{14},	Img_{15},	Img_{16}
$D_h \in \mathbb{R}^{512\times100}$	33.45	29.55	28.71	26.46	27.70	27.84	29.68	32.11
	0.8728	0.8298	0.6911	0.6534	0.6953	0.7154	0.7102	0.8617
$D_h \in \mathbb{R}^{1024\times100}$	36.96	32.90	31.13	31.41	30.18	31.69	30.40	33.89
	0.8883	0.8454	0.7241	0.7500	0.7149	0.7948	0.7279	0.8821
$D_h \in \mathbb{R}^{2048\times100}$	42.19	37.65	36.77	36.85	40.33	40.97	39.58	42.01
	0.9431	0.9296	0.8749	0.8483	0.9502	0.9490	0.9244	0.9969

From the performance, as shown in Table 3 using different dictionary pairs on Fig. 6 for electrical circuit, mechanical, civil and architectural design images and also from the Table. 3, it is observed that for dictionary pair ($\mathcal{D}_h \in \mathbb{R}^{25\times2048}$, $\mathcal{D}_l \in \mathbb{R}^{100\times2048}$) produces slightly better reconstructed SR images. For further comparison

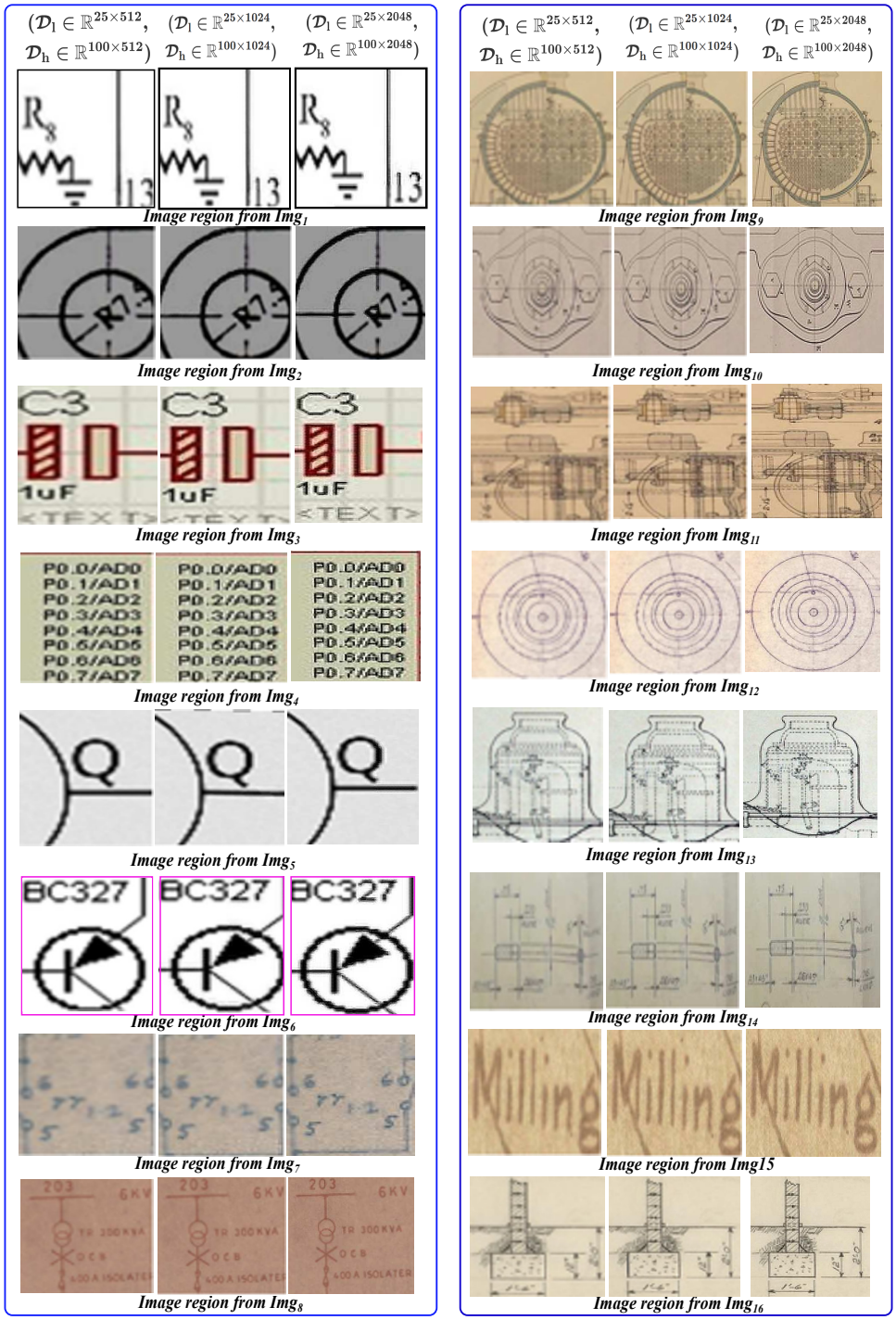

Figure 6: Performance of the proposed SR technique using the dictionary pair ($\mathcal{D}_l \in \mathbb{R}^{25\times512}$, $\mathcal{D}_h \in \mathbb{R}^{100\times512}$), ($\mathcal{D}_l \in \mathbb{R}^{25\times1024}$,$\mathcal{D}_h \in \mathbb{R}^{100\times1024}$) and ($\mathcal{D}_l \in \mathbb{R}^{25\times2048}$, $\mathcal{D}_h \in \mathbb{R}^{100\times2048}$ respectively.

of the proposed system with other competing methods such as Bicubic-Interpolation, Zhang et al. [28], Marquina et al. [14], Purkait et al. [19] and Yang et al. [26], we have employed ($\mathcal{D}_l \in \mathbb{R}^{25\times2048}$, $\mathcal{D}_h \in \mathbb{R}^{100\times2048}$)

dictionary pair. Here both visual perception analysis (Fig. 7 and Fig. 8) and the quantitative measures PSNR and SSIM (Table 4) have been employed with the reconstructed SR image obtained from the competing method and the proposed one. The performance of the proposed system with respect to visual information fidelity (VIF) evaluation index [30] has also been reported in Table 4 (Third row) along with the PSNR and SSIM indexes. The performance comparison with respect to these indexes show the superority of the proposed system.

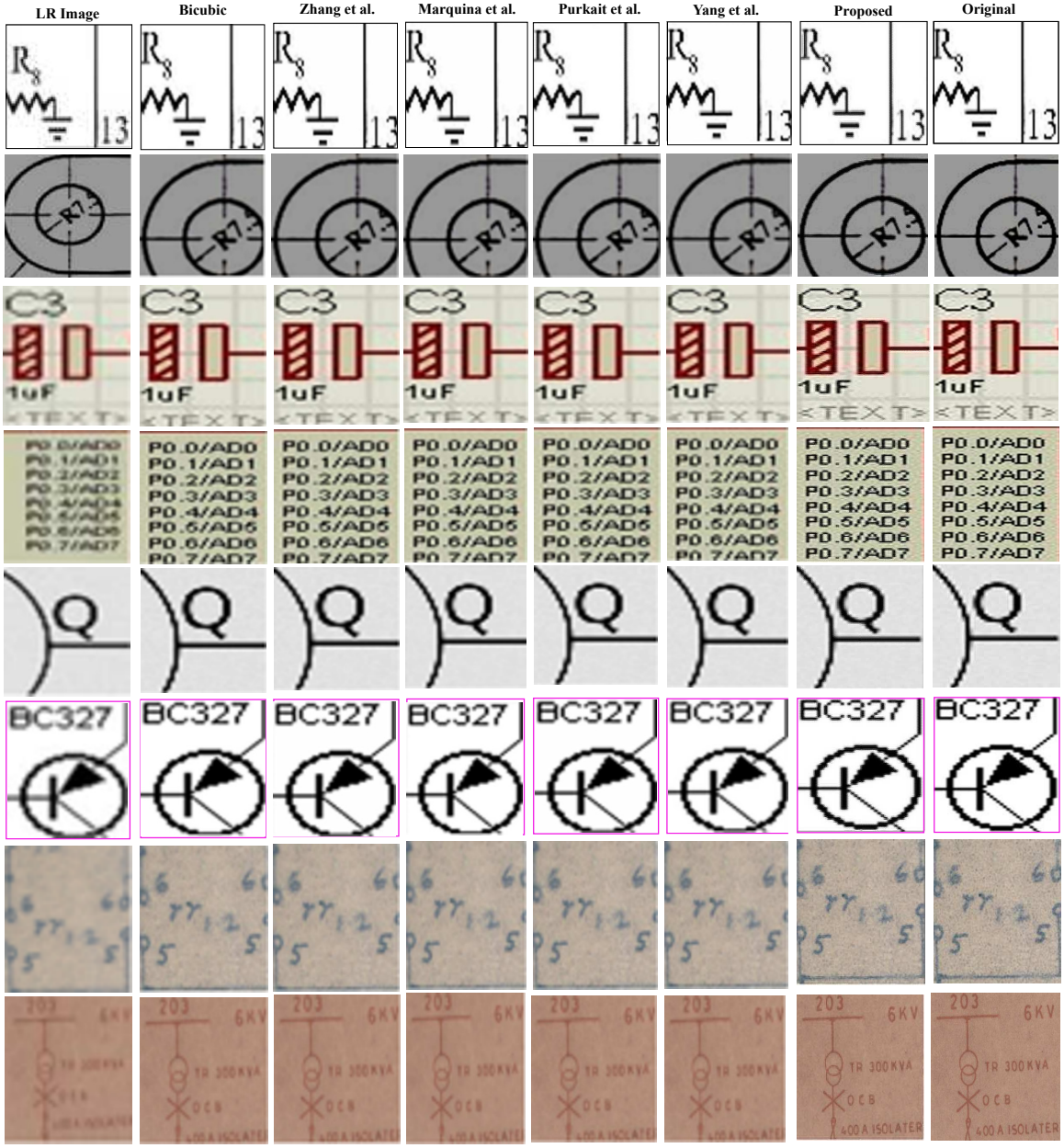

Figure 7: Performance comparison of the proposed SR technique with the other existing state-of-the-art methods for Img_1, Img_2, Img_3, Img_4, Img_5, Img_6, Img_7 and Img_8 respectively.

Bicubic-Interpolation is widely used for data interpolation on the two-dimensional regular grid. It is rela-

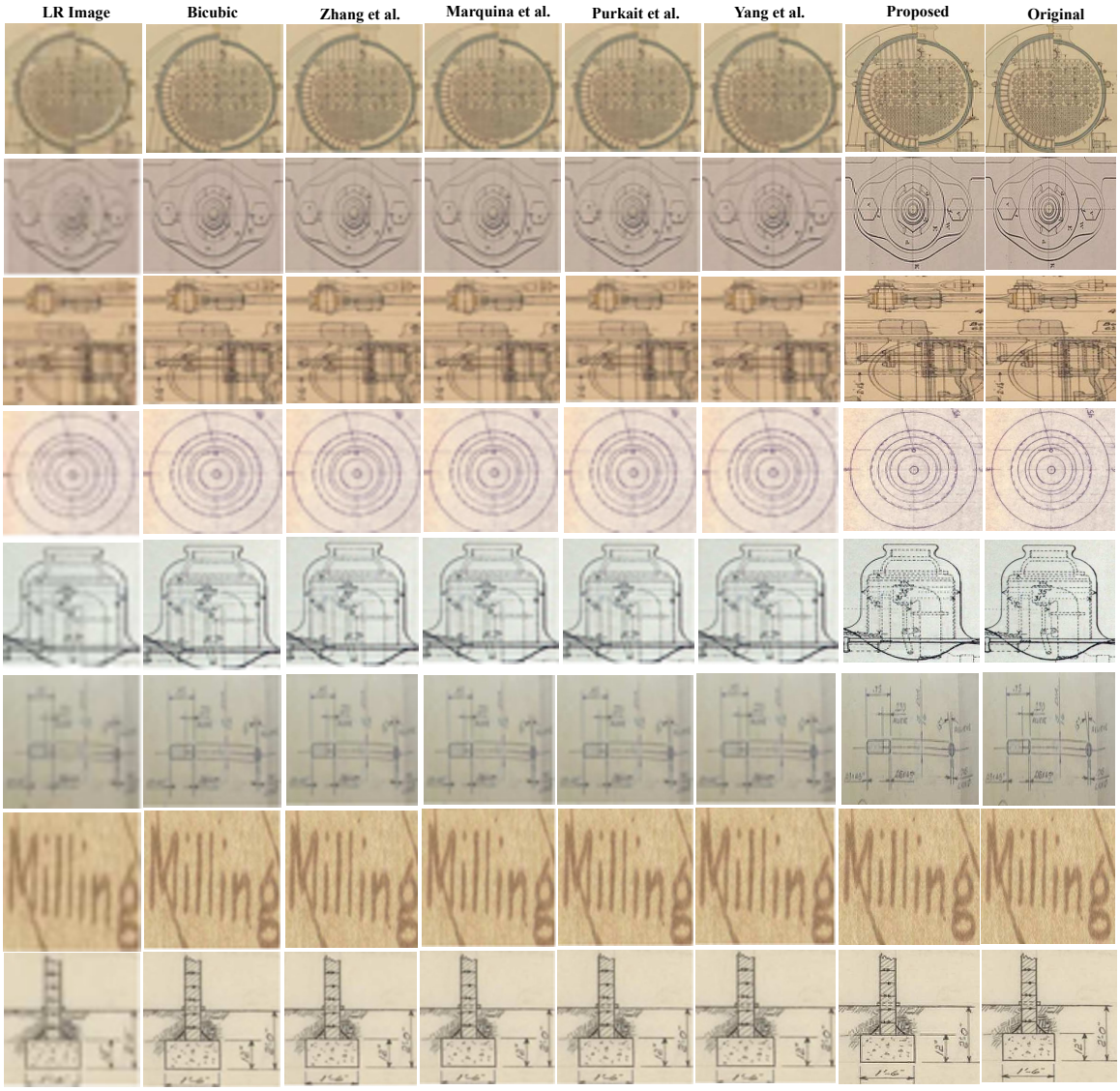

Figure 8: Performance comparison of the proposed SR technique with the other existing state-of-the-art methods for Img_9, Img_{10}, Img_{11}, Img_{12}, Img_{13}, Img_{14}, Img_{15} and Img_{16} respectively.

tively standard technique in the field of image interpolation with good results and low complexity. Zhang et al. [28] have given the empirical studies on the sensitivity of different single image super resolution algorithms based on different bluring kernels. Marquina et al. [14] proposed a convolutional model that uses the total variation of the signal followed by Bregman iterative refinement procedure for single image super resolution. Purkait et al. [19] had modeled a nonlinear regularization method based on multiscale morphology for reserving the edges for super resolution (SR) image reconstruction. Finally, Yang et al. [26] had proposed image super resolution method using sparse representation technique only where the sparse representation for each low resolution patch was used to get its coefficient as representation to obtain the corresponding high resolution

Table 4: Performance comparison of the proposed SR technique with the other existing techniques with respect to PSNR (First-rows), SSIM (Second-rows), and VIF (Third-rows) indexes.

	Img_1	Img_2	Img_3	Img_4	Img_5	Img_6	Img_7	Img_8
Bicubic	34.83	38.02	39.36	36.36	37.81	37.22	35.86	40.29
	0.9992	0.9997	0.9993	0.9986	0.9925	0.9947	0.9991	0.99917
	0.4758	0.4477	0.4359	0.4623	0.4496	0.4547	0.4667	0.4278
Zhang et al.[28]	37.68	37.70	34.75	32.72	35.66	36.73	32.81	36.88
	0.9422	0.9656	0.9060	0.9021	0.8927	0.8652	0.9687	0.9769
	0.4507	0.4505	0.4765	0.4943	0.4685	0.4591	0.4935	0.4577
Marquina et al. [14]	41.36	45.77	43.25	38.76	38.55	38.16	35.92	39.82
	0.9999	0.9997	0.9995	0.9993	0.9974	0.9997	0.9993	0.9993
	0.4184	0.3796	0.4017	0.4412	0.4431	0.4465	0.4662	0.4319
Purkait et al. [19]	38.00	45.04	42.99	39.07	39.15	36.54	37.29	40.90
	0.9999	0.9997	0.9997	0.9997	0.9980	0.9998	0.9997	0.9997
	0.4479	0.386	0.404	0.4385	0.4378	0.4607	0.4541	0.4224
Yang et al. [26]	37.32	43.58	35.72	38.51	33.71	33.81	34.24	39.69
	0.9994	0.9993	0.9972	0.9969	0.9910	0.9921	0.9972	0.9981
	0.4539	0.3988	0.4679	0.4434	0.4856	0.4847	0.4809	0.433
Proposed	40.84	46.52	39.89	38.63	38.89	37.59	36.51	40.11
	0.9994	0.9999	0.9987	0.9982	0.9915	0.9928	0.9990	0.9991
	0.5907	0.5957	0.5899	0.5888	0.589	0.5879	0.5869	0.5901
	Img_9	Img_{10}	Img_{11}	Img_{12}	Img_{13}	Img_{14}	Img_{15}	Img_{16}
Bicubic	30.08	32.09	31.44	31.09	33.87	31.41	29.17	33.89
	0.8986	0.9170	0.9276	0.8725	0.8959	0.8991	0.8276	0.8951
	0.5175	0.4998	0.5056	0.5086	0.4842	0.5058	0.5255	0.484
Zhang et al.[28]	33.86	32.95	32.33	33.52	32.83	32.01	33.18	33.56
	0.9666	0.9505	0.9089	0.8873	0.8280	0.9391	0.9030	0.9254
	0.4843	0.4923	0.4977	0.4873	0.4933	0.5005	0.4903	0.4869
Marquina et al. [14]	39.67	33.06	29.64	29.42	32.18	33.53	34.57	36.50
	0.9983	0.8170	0.7969	0.7880	0.8143	0.8290	0.8978	0.9356
	0.4332	0.4913	0.5214	0.5233	0.4991	0.4872	0.4780	0.4611
Purkait et al. [19]	37.95	36.02	32.39	32.59	35.80	37.55	34.05	36.67
	0.8995	0.8796	0.8491	0.8234	0.8926	0.8693	0.8494	0.9278
	0.4483	0.4653	0.4972	0.4955	0.4672	0.4518	0.4826	0.4596
Yang et al. [26]	33.05	33.43	36.28	32.05	32.18	33.43	37.25	37.65
	0.8960	0.8931	0.8901	0.8385	0.8212	0.8492	0.8651	0.8835
	0.5053	0.5023	0.4797	0.5132	0.5121	0.5023	0.472	0.4689
Proposed	42.19	37.65	36.77	36.85	40.33	40.97	39.58	42.01
	0.9431	0.9796	0.9249	0.8983	0.9502	0.9490	0.9244	0.9969
	0.5919	0.5879	0.5871	0.5872	0.5903	0.5908	0.5896	0.5917

patch. From the Fig. 7 and Fig. 8 it has been shown that the proposed system applied on images, have better reconstructed.

Here the Table 5 shows the comparison performance with respect to time in *Sec.*. Since the proposed system and method in [19] outperforms other competing methods. Additionally, the performance of the proposed method and method in [19] are more or less the same even in some circumstances. It has been observed that for some images, the proposed system overcomes [19]. But due to some experimental setup and might be in some

Table 5: Average performance of the competing methods & the proposed system in terms of time (Sec.).

Name	Time (Sec.)
Zhang et al.[28]	10.82
Marquina et al. [14]	08.12
Purkait et al. [19]	07.11
Yang et al. [26]	10.24
Proposed	07.31

tuning of parameters, the proposed system will take lesser time than [19]. Moreover, the performance reported in Table 4, it has been observed that the proposed system gives outstanding performance in terms of PSNR, SSIM, and VIF as compared to the methods reported in Table 5. Hence, the proposed system outperforms other competing methods.

5. Conclusions

This paper presents a novel method of single image super-resolution technique. The proposed scheme has three components. In the first component, to speed up the process, the input image is divided into several regions, analyzed into homogeneous or non-homogeneous regions based on the texture pattern analysis in those regions. In the second component, the non-homogeneous region undergoes a sparse representation technique to get a better-reconstructed HR region. In the third component, the reconstructed HR region from the second component undergoes a prediction model based on the statistical modeling of sparse representation using the Boltzmann machine technique to get a more enhanced reconstructed HR image. The homogeneous regions are bicubic interpolated and reflected the outcome image. Experimental results demonstrate that the proposed method better reconstructed SR images for electrical, machine, and civil design images. The comparison with the existing state-of-the-art methods shows that the proposed system outperforms other methods with efficient time. For the larger scaled images, the proposed system might take some time to generate its super-resolution images. In the future, some deep learning models will be employed to solve super-resolution problems for the vast scaled engineering design images.

Data Availability

All data needed to evaluate the experimentation in the paper are present in the paper or the references cited here within.

Conflicts of Interest

Authors declare that they have no conflicts of interest.

Acknowledgment

This work was supported by the Researchers Supporting Project (No. RSP-2021/395), King Saud University, Riyadh, Saudi Arabia

Author contributions:

Ramanath Datta: Data curation, Visualization; Shekhar Mandal: Conceptualization; Saiyed Umer: Methodology, Implementation, Writing Original draft preparation, Investigation; Ahmad Ali AlZubi: Supervision; Abdullah Alharbi: Software, Validation; Jazem Mutared Alanazi : Writing- Reviewing and Editing.

,

References

[1] Michal Aharon, Michael Elad, Alfred Bruckstein, et al. K-svd: An algorithm for designing overcomplete dictionaries for sparse representation. *IEEE Transactions on signal processing*, 54(11):4311, 2006.

[2] AydıN Akyol and Muhittin GöKmen. Super-resolution reconstruction of faces by enhanced global models of shape and texture. *Pattern Recognition*, 45(12):4103–4116, 2012.

[3] Leonard E Baum and John Alonzo Eagon. An inequality with applications to statistical estimation for probabilistic functions of markov processes and to a model for ecology. *Bulletin of the American Mathematical Society*, 73(3):360–363, 1967.

[4] Feilong Cao and Keqiuyin Li. A new method for image super-resolution with multi-channel constraints. *Knowledge-Based Systems*, 146:118–128, 2018.

[5] Hong Chang, Dit-Yan Yeung, and Yimin Xiong. Super-resolution through neighbor embedding. In *Computer Vision and Pattern Recognition, 2004. CVPR 2004. Proceedings of the 2004 IEEE Computer Society Conference on*, volume 1, pages I–I. IEEE, 2004.

[6] Shengyang Dai, Mei Han, Wei Xu, Ying Wu, and Yihong Gong. Soft edge smoothness prior for alpha channel super resolution. In *Computer Vision and Pattern Recognition, 2007. CVPR'07. IEEE Conference on*, pages 1–8. IEEE, 2007.

[7] Chinh Dang and Hayder Radha. Fast single-image super-resolution via tangent space learning of high-resolution-patch manifold. *IEEE Transactions on Computational Imaging*, 3(4):605–616, 2017.

[8] William T Freeman, Egon C Pasztor, and Owen T Carmichael. Learning low-level vision. *International journal of computer vision*, 40(1):25–47, 2000.

[9] Daniel Glasner, Shai Bagon, and Michal Irani. Super-resolution from a single image. In *Computer Vision, 2009 IEEE 12th International Conference on*, pages 349–356. IEEE, 2009.

[10] Takayuki Honda, Takayuki Hamamoto, and Daisuke Sugimura. Low-light color image super-resolution using rgb/nir sensor. In *2018 25th IEEE International Conference on Image Processing (ICIP)*, pages 56–60. IEEE, 2018.

[11] Alain Hore and Djemel Ziou. Image quality metrics: Psnr vs. ssim. In *Pattern recognition (icpr), 2010 20th international conference on*, pages 2366–2369. IEEE, 2010.

[12] Jung Woo Hwang and Hwang Soo Lee. Adaptive image interpolation based on local gradient features. *IEEE Signal Processing Letters*, 11(3):359–362, 2004.

[13] Rui Lai, Yin-tang Yang, Hui-xin Zhou, Han-lin Qin, and Bing-jian Wang. Total variation regularized iterative back-projection method for single frame image super resolution. In *Signal Processing (ICSP), 2012 IEEE 11th International Conference on*, volume 2, pages 931–934. IEEE, 2012.

[14] Antonio Marquina and Stanley J Osher. Image super-resolution by tv-regularization and bregman iteration. *Journal of Scientific Computing*, 37(3):367–382, 2008.

[15] Peyman Milanfar. *Super-resolution imaging*. CRC press, 2010.

[16] Yusuke Natsui and Tomoharu Nagao. Single frame super-resolution using multiple graph structured program. In *Computational Intelligence and Applications (IWCIA), 2016 IEEE 9th International Workshop on*, pages 75–80. IEEE, 2016.

[17] Kien Nguyen, Clinton Fookes, Sridha Sridharan, Massimo Tistarelli, and Mark Nixon. Super-resolution for biometrics: A comprehensive survey. *Pattern Recognition*, 78:23–42, 2018.

[18] Tomer Peleg and Michael Elad. A statistical prediction model based on sparse representations for single image super-resolution. *IEEE transactions on image processing*, 23(6):2569–2582, 2014.

[19] Pulak Purkait and Bhabatosh Chanda. Super resolution image reconstruction through bregman iteration using morphologic regularization. *IEEE Transactions on Image Processing*, 21(9):4029–4039, 2012.

[20] Yuexia Shu, Changpeng Han, Minglei Lv, and Xin Liu. Fast super-resolution ultrasound imaging with compressed sensing reconstruction method and single plane wave transmission. *IEEE Access*, 6:39298–39306, 2018.

[21] Jian Sun, Zongben Xu, and Heung-Yeung Shum. Image super-resolution using gradient profile prior. In *Computer Vision and Pattern Recognition, 2008. CVPR 2008. IEEE Conference on*, pages 1–8. IEEE, 2008.

[22] Ilya Sutskever, Geoffrey E Hinton, and Graham W Taylor. The recurrent temporal restricted boltzmann machine. In *Advances in neural information processing systems*, pages 1601–1608, 2009.

[23] Farzad Toutounchi, Valia Guerra Ones, and Ebroul Izquierdo. An efficient video super-resolution approach based on sparse representation. In *Multimedia Signal Processing (MMSP), 2017 IEEE 19th International Workshop on*, pages 1–6. IEEE, 2017.

[24] Saiyed Umer, Bibhas Chandra Dhara, and Bhabatosh Chanda. Texture code matrix-based multi-instance iris recognition. *Pattern Analysis and Applications*, 19(1):283–295, 2016.

[25] John Wright, Yi Ma, Julien Mairal, Guillermo Sapiro, Thomas S Huang, and Shuicheng Yan. Sparse representation for computer vision and pattern recognition. *Proceedings of the IEEE*, 98(6):1031–1044, 2010.

[26] Jianchao Yang, John Wright, Thomas S Huang, and Yi Ma. Image super-resolution via sparse representation. *IEEE transactions on image processing*, 19(11):2861–2873, 2010.

[27] Jianchao Yang, Zhaowen Wang, Zhe Lin, Scott Cohen, and Thomas Huang. Coupled dictionary training for image super-resolution. *IEEE transactions on image processing*, 21(8):3467–3478, 2012.

[28] Kai Zhang, Xiaoyu Zhou, Hongzhi Zhang, and Wangmeng Zuo. Revisiting single image super-resolution under internet environment: blur kernels and reconstruction algorithms. In *Pacific Rim Conference on Multimedia*, pages 677–687. Springer, 2015.

[29] Jianwei Zhao, Heping Hu, and Feilong Cao. Image super-resolution via adaptive sparse representation. *Knowledge-Based Systems*, 124:23–33, 2017.

[30] Tien-Ying Kuo, Po-Chyi Su, and Cheng-Mou Tsai. Improved visual information fidelity based on sensitivity characteristics of digital images. *Journal of visual communication and image representation*, 40:76–84, 2016.